Hindawi Publishing Corporation
International Journal of Photoenergy
Volume 2014, Article ID 639509, 5 pages
http://dx.doi.org/10.1155/2014/639509

*Research Article*

# Origin of Visible Light Photocatalytic Activity of $Ag_3AsO_4$ from First-Principles Calculation

**Yan Gong, Hongtao Yu, and Xie Quan**

*Key Laboratory of Industrial Ecology and Environmental Engineering of Ministry of Education, School of Environmental Science and Technology, Dalian University of Technology, Dalian 116024, China*

Correspondence should be addressed to Xie Quan; quanxie@dlut.edu.cn

Received 12 December 2013; Revised 18 February 2014; Accepted 4 March 2014; Published 21 May 2014

Academic Editor: Yuexiang Li



Recently a novel sliver oxide $Ag_3AsO_4$ has been found to be an excellent photocatalyst with strong oxidation capability for pollutant degradation under visible light. But the origin of its high visible light photocatalytic activity was unclear which hindered further research of $Ag_3AsO_4$. For clarifying that, the electronic structure and optical properties of $Ag_3AsO_4$ have been analyzed by the hybrid density functional method. The results reveal that the $Ag_3AsO_4$ presents a narrow band gap with strong oxidation ability of the valence bands maximum edge and the highly delocalized charge distribution of the conduction bands minimum is beneficial for the carriers transfer to surface to participate in the photocatalytic reaction. These results provide clear explanations of the excellent visible light photocatalytic performance of the $Ag_3AsO_4$ from microscopic aspect. And it is significant to design novel materials with high photocatalytic performance.

## 1. Introduction

Semiconductor photocatalysts are finding increasing applications in high-efficiency solar cells [1], water/air purification [2], and water splitting [3, 4]. For the purpose of effectively utilizing solar energy, ideal semiconductor photocatalysts should at least have the two characteristics. One important aspect is a narrow band gap for utilizing the visible light which dominates 43% of the solar light and almost 100% of indoor light. The other one is a suitable band edge position for water splitting and environment pollutants decomposition or other target reactions. In the past decades, overwhelming attention has focused on designing visible-light response photocatalysts, such as $BiVO_4$ [5], CdS [6], and $WO_3$ [7]. However, their low visible-light photocatalytic activity is of course a great inhibition to use as a highly efficient photocatalysts.

Since Yi's group has reported the strong oxidation power of $Ag_3PO_4$ under visible light [8], a series of sliver based oxides has aroused wide attention on account of their excellent photocatalytic abilities under visible light region, such as $Ag_3VO_4$ [9], $AgSbO_3$ [10], and $Ag_2O$ [11]. Among them, as a novel sliver oxide photocatalyst, $Ag_3AsO_4$, has been found to be an excellent photocatalyst with powerful oxidation ability under visible light by Tang's group recently [12]. It has a band gap of 1.6 eV which can fulfill the high absorption capacity of visible light. And the potential of valence band edge is about 2.22 eV that the photogenerated holes own strong oxidation to decompose the pollutants efficiently. Despite important insight being achieved, the mechanisms involved in photocatalysis are not yet clear. Fulfilling this goal requires the assistance of theoretical investigations such as electronic structure calculations. Therefore, a systemic investigation about microscopic mechanism of photocatalysis is vitally important for understanding the excellent photocatalytic performance of $Ag_3AsO_4$.

To understand the superior photocatalytic activity of $Ag_3AsO_4$ from its intrinsic properties, the first-principles calculations on its electronic structure and optical properties were carried out in our work. As a common problem, the band gaps of the semiconductors are usually underestimated by the conventional DFT methods due to the self-interaction error as well as the missing discontinuity in the exchange-correlation potential. For instance, the band gap error exceeds 2 eV for ZnO [13, 14] and $Ag_3PO_4$ [15]. This is adverse to analysis of the redox ability of the semiconductor.

The hybrid-DFT with PBE0 formalism has been successfully used as an available method to calculate the band gap accurately, such as $Ag_3PO_4$ [16]. So in our work, the hybrid-DFT method PBE0 was applied to calculate the electronic structures and optical properties. The results revealed that the hybrid-DFT method is more precise for the calculation of the electronic and band structures of $Ag_3AsO_4$. Furthermore, we analyzed the relations of these microscopic factors to photocatalytic activities of $Ag_3AsO_4$.

## 2. Computational Methods

In this paper, our first-principles calculations were performed using the plane-wave pseudopotential method based on hybrid-DFT with PBE0 formalism, which was implemented in the CASTEP code [17]. Three-dimensional periodic boundary conditions were employed to simulate an infinite solid. The generalized gradient approximation (GGA) in the PBE0 hybrid functional formalism was applied combined with norm-conserving pseudopotentials. To achieve the accurate density of the electronic states, a $4 \times 4 \times 4$ Monkhorst-Pack grid [18] was used for Brillouin-zone sampling. A plane-wave basis set with a cutoff of 400 eV was used. Geometric optimization was achieved and the convergence criterion for the force between atoms was $3 \times 10^{-2}$ eV/Å, the maximum displacement was $1 \times 10^{-3}$ Å, and the total energy and the maximal stress were $1 \times 10^{-5}$ eV/atom and $5 \times 10^{-2}$ GPa, respectively. The self-consistent convergence accuracy was set at $1.0 \times 10^{-6}$ eV/atom, and the valence configurations of the pseudopotentials are $4d^{10}5s^1$ for Ag, $4s^24p^3$ for As, and $2s^22p^4$ for O, respectively.

## 3. Results and Discussion

*3.1. Geometry Structure and Bonding Character.* The geometry optimization crystal structure of $Ag_3AsO_4$ is a cubic structure with P4-3n symmetry which is shown in Figures 1(a) and 1(b). Figure 1(b) presents the polyhedron configurations of the $Ag_3AsO_4$. It clearly shows that both the silver and arsenic atoms are coordinated to four oxygen atoms forming $AgO_4$ and $AsO_4$ tetrahedral units, respectively. The optimized cell parameters are $a = b = c = 6.22$ Å and $a = b = c = 90^\circ$ and agree well with the experimental data of $a = b = c = 6.12$ Å and $a = b = c = 90^\circ$ [19]. The deviations are less than 1.6% that indicates the accuracy of our calculation. The As–O and Ag–O bond length are calculated to be 1.717 Å and 2.408 Å, respectively. To understand the nature of the chemical bonding behavior, a Mulliken bond population analysis is used. Generally, bond population is a common characteristic used to analyze ionic and covalent characters. When the value of bond population is close to zero, it presents an ideal ionic bond, while higher value demonstrates higher covalent interactions. The result indicates that the As–O bond population is 0.55, and the Ag–O is 0.17. Therefore, the interaction between arsenic and oxygen is achieved mainly by covalent bond, while the interaction between silver and oxygen is formed mainly by ionic bond. Previous study showed that the short Ag–Ag distance results in the formation of the metallic Ag–Ag bond, which contributes to the dispersive conduction bands and a small effective mass of electron [20]. The length of Ag–Ag bond is 3.112 Å which is much smaller than that in $Ag_2O$ (3.30 Å) and $AgNbO_3$ (3.90 Å), but a little larger than $AgPO_3$ (2.95 Å). So the shorter Ag–Ag distance in the $Ag_3AsO_4$ indicates the metallic Ag–Ag bond which has remarkable influence of the band structure of the $Ag_3AsO_4$.

*3.2. Band Structures and Density of States.* The band structures of $Ag_3AsO_4$ determined by PBE0 are shown in Figure 2. The Fermi level (indicated by dashed line) is set as zero. The conduction bands minimum (CBM) is at G point and the valence bands maximum (VBM) is located at M point in the Brillouin zone illustrated in Figure 2. It indicates that $Ag_3AsO_4$ is an indirect band gap semiconductor. The indirect gap from M to G is calculated to be 1.67 eV and the direct gap at G is 1.80 eV. The hybrid-DFT method (PBE0) gives a much more credible band gap of 1.67 eV, which agrees well with the experimental value (1.6 eV). From this figure, the bottom of conduction band shows well dispersive, compared with the top of valence band, which manifests that the photogenerated electrons possess smaller effective mass. In general, a lower carrier effective mass corresponds to a higher carrier mobility. So the photogenerated electrons in the conduction band can transfer more rapidly to the surface of $Ag_3AsO_4$ to participate in the photocatalytic reaction.

In order to better understand the nature of the electronic band structures, the density of total states (TDOS) of $Ag_3AsO_4$ and projected density of states (PDOS) for Ag, As, and O elements calculated by PBE0 are presented in Figure 3. The valence bands are mainly occupied by O 2p and Ag 4d states. Meanwhile, above the Fermi level, the conduction bands are composed of Ag 5s and Ag 5p. As shown in Figure 3, there are no Ag d states in the CBM of the $Ag_3AsO_4$. This character is beneficial for the transfer of photogenerated electrons in the CBM, due to the fact that Ag sp states are less localized than Ag d states. Thus the photogenerated electrons in the CBM of $Ag_3AsO_4$ can be rapidly transferred to the surface to participate in the reaction. This gives a further detailed explanation of the high photocatalytic performance of the $Ag_3AsO_4$.

*3.3. Redox Potentials.* In addition to a narrow band gap and low recombination rate of photogenerated carriers, suitable redox potentials are also integrant for an ideal visible-light driven photocatalyst. The redox ability is evaluated by aligning the VBM and CBM with respect to the water oxidation/reduction potential level. Generally, the more positive VBM corresponds to the higher photooxidation potential of the photogenerated holes, while the more negative potentials of the CBM reflect the stronger reduction ability of the photogenerated electrons. The positions can be theoretically

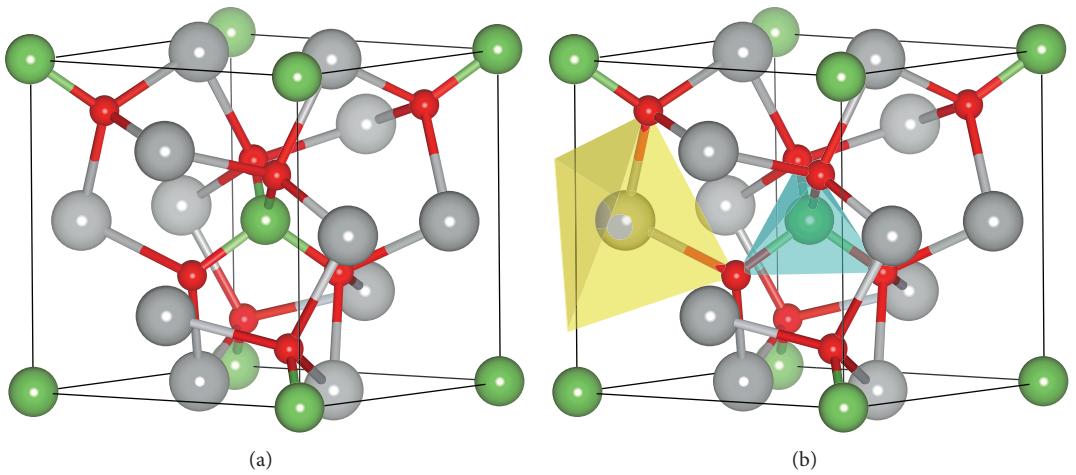


FIGURE 1: Crystal structure of $Ag_3AsO_4$ with P4-3n space group (a) ball and stick and (b) polyhedron configurations. Red, green, and gray spheres represent O, As, and Ag atoms. $AgO_4$ and $AsO_4$ tetrahedral units are indicated by the yellow and blue tetrahedrons, respectively.

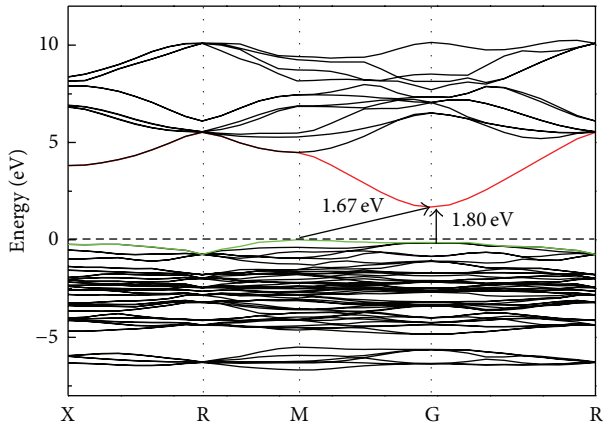


FIGURE 2: Band structure of $Ag_3AsO_4$ calculated using the PBE0 approach.

predicted according to the equation as follows using Mulliken electronegativity and the value of band gap:

$$E_{CB} = X - E_e - \frac{1}{2}E_g$$
$$E_{VB} = E_{CB} + E_g, \quad (1)$$

where $E_{CB}$ and $E_{VB}$ are the CB and VB edge potential, respectively and $X$ is the Mulliken electronegativity of $Ag_3AsO_4$. The Mulliken electronegativity of a semiconductor is the geometric mean of the electronegativities of the constituent atoms, and the Mulliken electronegativity of an atom is the arithmetic mean of the atomic electron affinity and the first ionization energy [21]. The calculated $X$ is 5.92 eV. $E_e$ is the energy of free electrons on the hydrogen scale (4.5 eV) and $E_g$ is the band gap from PBE0 approach. The corresponding valence and conduction band edge potentials of $Ag_3AsO_4$ are shown in Figure 4. $Ag_3AsO_4$ presents positive CBM potential (0.59 V versus NHE) and thus cannot reduce $H^+$ to $H_2$ in water from thermodynamics aspect. Meanwhile the VBM potential is 2.26 V which is more positive than $O_2/H_2O$ (1.23 V). For the band edge position of the $Ag_3AsO_4$, no experiment value is reported and the only calculation result from reference is 2.22 V for $E_{VB}$ and 0.62 V for $E_{CB}$ [12]. These values are very close to our calculated result, and the error is less than 1%. It indicates that this method is suitable for calculating the band edge position of the semiconductors. In fact, the error is associated with the derivative discontinuity of the exchange-correlation energy [22]. The $Ag_3AsO_4$ can decompose most of refractory organics into readily biodegradable compounds and eventually mineralized them to carbon dioxide and water by the strong oxidation ability of the photogenerated holes under visible light irradiation.

*3.4. Optical Absorption.* Because the optical adsorption property of semiconductors has a great affinity to their photocatalytic properties, it is very necessary to investigate their optical adsorption properties. In general, the optical absorption property of the solid can be described by the dielectric function $\varepsilon = \varepsilon_1(\omega) + i\varepsilon_2(\omega)$, where $\varepsilon_1(\omega)$ and $\varepsilon_2(\omega)$ are the real part and the imaginary part of the dielectric function, respectively. The $\varepsilon_2(\omega)$ can be obtained from the momentum matrix elements between the occupied and unoccupied wave functions as [23–25]

$$\varepsilon_2(\omega) = \frac{2e^2\pi}{\Omega\varepsilon_0}\sum_{k,v,c}\left|\left\langle\psi_k^c\left|ur\right|\psi_k^v\right\rangle\right|^2\delta\left(E_k^c - E_k^v - E\right), \quad (2)$$

where $\Omega$ is the volume of the elementary cell, $\omega$ is the frequency of the incident photon, $e$ refers to electron charge, and $\psi^c$ and $\psi^v$ are the CB and VB wave functions at $k$, respectively. And the real part $\varepsilon_1(\omega)$ is determined from $\varepsilon_2(\omega)$ via a Kramers-Kronig transform. The calculated optical absorption spectrum of $Ag_3AsO_4$ is presented in Figure 5. It can be obtained base on calculating the imaginary part of the dielectric function using (2). The optical adsorption calculation is performed using the "polycrystalline" polarization where the $E$ field vector is an isotropic average over

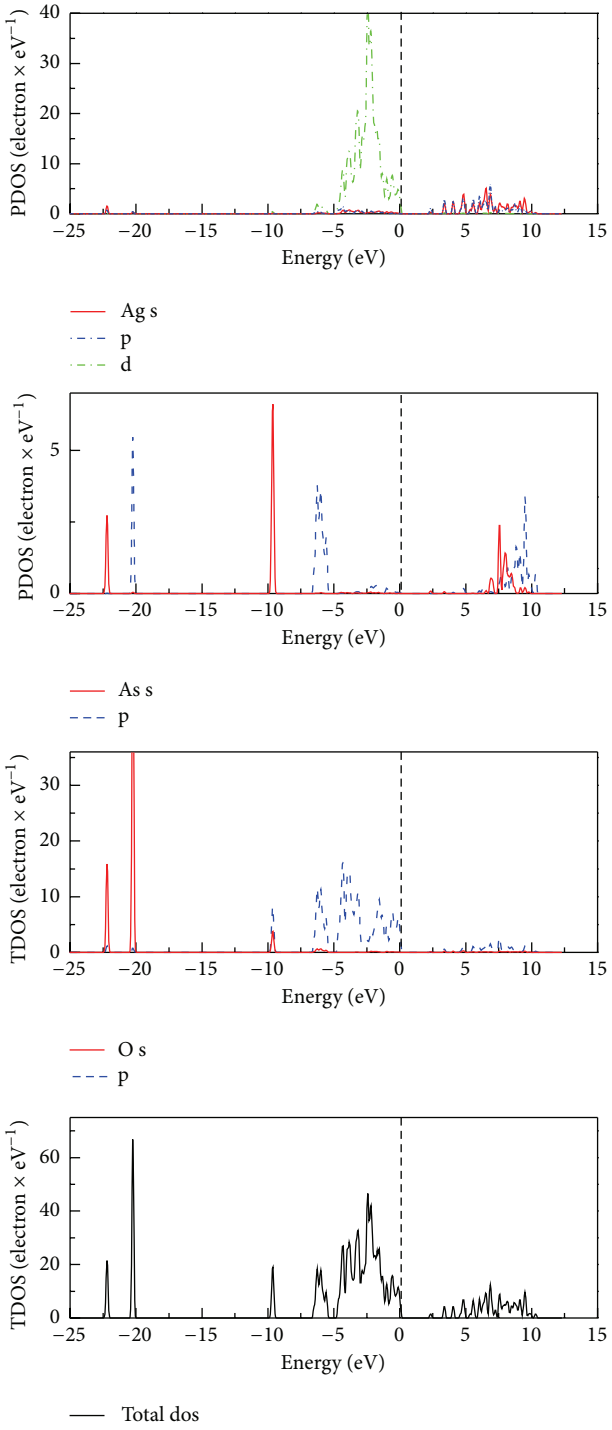


Figure 3: TDOS and PDOS of $Ag_3AsO_4$ using PBE0 approach.

all directions. In order to better distinguish the absorption peaks, a small smearing of 0.1 eV is applied. As shown in Figure 5, the curve starts at about 550 nm with the first intensive peak at wavelength about 510 nm. This peak is contributed by the phototransition energies from the VBM to the CB under visible-light irradiation, indicating that $Ag_3AsO_4$ is a visible-light-response photocatalyst.

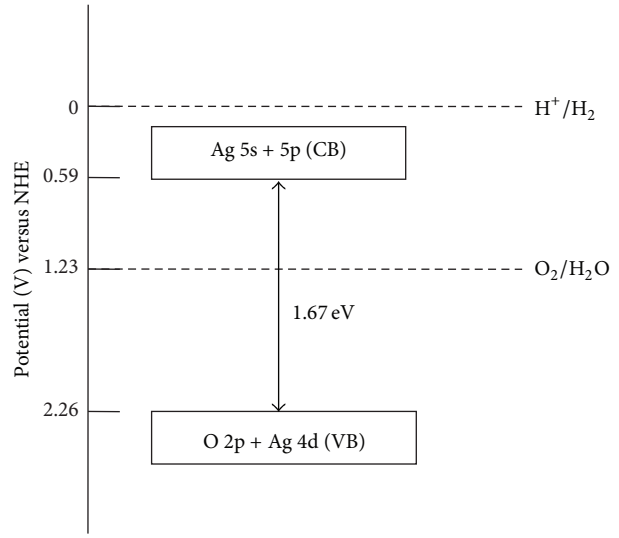


Figure 4: The calculated CBM and VBM potentials of $Ag_3AsO_4$.

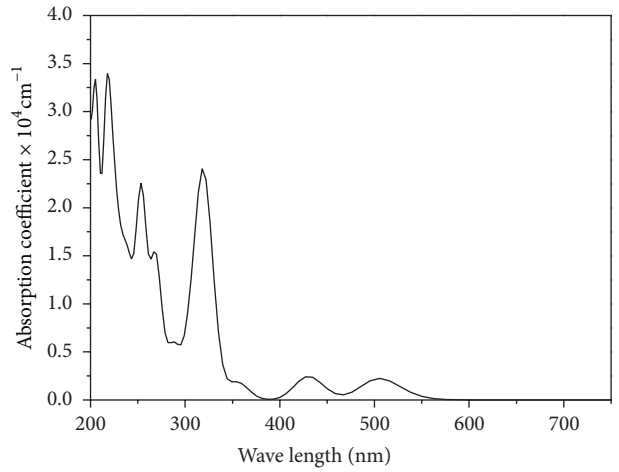


Figure 5: Calculated absorption coefficient of $Ag_3AsO_4$.

## 4. Conclusions

In summary, we studied the electronic structure and optical properties of $Ag_3AsO_4$ by hybrid density functional method. The origin of the excellent visible light photocatalytic activity of $Ag_3AsO_4$ is attributed to the highly dispersive band structure of the CBM resulting from Ag s-Ag p hybridization without localized d states and the narrow band gap with a strong oxidation ability of the VBM edge. The calculation results can raise the level of understanding and provide guidance toward the practical improvement of photocatalytic materials and their applications.

## Conflict of Interests

The authors declare that there is no conflict of interests regarding the publication of this paper.

## Acknowledgment

This work was supported by the National Natural Science Foundation of China (NSFC-JST 21261140334).

## References

[1] A. Fujishima and K. Honda, "Electrochemical photolysis of water at a semiconductor electrode," *Nature*, vol. 238, no. 5358, pp. 37–38, 1972.

[2] M. N. Chong, B. Jin, C. W. K. Chow, and C. Saint, "Recent developments in photocatalytic water treatment technology: a review," *Water Research*, vol. 44, no. 10, pp. 2997–3027, 2010.

[3] X. Chen and S. S. Mao, "Titanium dioxide nanomaterials: synthesis, properties, modifications and applications," *Chemical Reviews*, vol. 107, no. 7, pp. 2891–2959, 2007.

[4] M. R. Hoffmann, S. T. Martin, W. Choi, and D. W. Bahnemann, "Environmental applications of semiconductor photocatalysis," *Chemical Reviews*, vol. 95, no. 1, pp. 69–96, 1995.

[5] S. S. Dunkle, R. J. Helmich, and K. S. Suslick, "$BiVO_4$ as a visible-light photocatalyst prepared by ultrasonic spray pyrolysis," *Journal of Physical Chemistry C*, vol. 113, no. 28, pp. 11980–11983, 2009.

[6] M. Matsumura, Y. Saho, and H. Tsubomura, "Photocatalytic hydrogen production from solutions of sulfite using platinized cadmium sulfide powder," *Journal of Physical Chemistry*, vol. 87, no. 20, pp. 3807–3808, 1983.

[7] H. Reiche, W. W. Dunn, and A. J. Bard, "Heterogeneous photocatalytic and photosynthetic deposition of copper on Titanium dioxide and tungsten(VI) oxide powder," *Journal of Physical Chemistry*, vol. 83, no. 17, pp. 2248–2251, 1979.

[8] Z. Yi, J. Ye, N. Kikugawa et al., "An orthophosphate semiconductor with photooxidation properties under visible-light irradiation," *Nature Materials*, vol. 9, no. 7, pp. 559–564, 2010.

[9] X. Hu, C. Hu, and J. Qu, "Preparation and visible-light activity of silver vanadate for the degradation of pollutants," *Materials Research Bulletin*, vol. 43, no. 11, pp. 2986–2997, 2008.

[10] T. Kako, N. Kikugawa, and J. Ye, "Photocatalytic activities of $AgSbO_3$ under visible light irradiation," *Catalysis Today*, vol. 131, no. 1–4, pp. 197–202, 2008.

[11] W. Zhou, H. Liu, J. Wang, D. Liu, G. Du, and J. Cui, "$Ag_2O/TiO_2$ nanobelts heterostructure with enhanced ultraviolet and visible photocatalytic activity," *ACS Applied Materials and Interfaces*, vol. 2, no. 8, pp. 2385–2392, 2010.

[12] J. Tang, Y. Liu, H. Li, Z. Tan, and D. Li, "A novel $Ag_3AsO_4$ visible-light-responsive photocatalyst: facile synthesis and exceptional photocatalytic performance," *Chemical Communications*, vol. 49, no. 48, pp. 5498–5500, 2013.

[13] S. Lany and A. Zunger, "Assessment of correction methods for the band-gap problem and for finite-size effects in supercell defect calculations: case studies for ZnO and GaAs," *Physical Review B: Condensed Matter and Materials Physics*, vol. 78, no. 23, Article ID 235104, 25 pages, 2008.

[14] A. Walsh, Y. Yan, M. N. Huda, M. M. Al-Jassim, and S.-H. Wei, "Band edge electronic structure of $BiVO_4$: elucidating the role of the Bi s and V d orbitals," *Chemistry of Materials*, vol. 21, no. 3, pp. 547–551, 2009.

[15] X. Ma, B. Lu, D. Li, R. Shi, C. Pan, and Y. Zhu, "Origin of photocatalytic activation of silver orthophosphate from first-principles," *Journal of Physical Chemistry C*, vol. 115, no. 11, pp. 4680–4687, 2011.

[16] J. J. Liu, X. L. Fu, S. F. Chen, and Y. F. Zhu, "Electronic structure and optical properties of $Ag_3PO_4$ photocatalyst calculated by hybrid density functional method," *Applied Physics Letters*, vol. 99, no. 19, Article ID 191903, 3 pages, 2011.

[17] M. D. Segall, P. J. D. Lindan, M. J. Probert et al., "First-principles simulation: ideas, illustrations and the CASTEP code," *Journal of Physics Condensed Matter*, vol. 14, no. 11, pp. 2717–2744, 2002.

[18] H. J. Monkhorst and J. D. Pack, "Special points for Brillouin-zone integrations," *Physical Review B*, vol. 13, no. 12, pp. 5188–5192, 1976.

[19] L. Helmholz, "A determination of parameters in potassium dihydrogen arsenate and silver arsenate," *Journal of the American Chemical Society*, vol. 64, no. 2, pp. 354–358, 1942.

[20] N. Umezawa, O. Shuxin, and J. Ye, "Theoretical study of high photocatalytic performance of $Ag_3PO_4$," *Physical Review B: Condensed Matter and Materials Physics*, vol. 83, no. 3, Article ID 035202, 8 pages, 2011.

[21] J. Liu, S. Chen, Q. Liu, Y. Zhu, and J. Zhang, "Correlation of crystal structures and electronic structures with visible light photocatalytic properties of $NaBiO_3$," *Chemical Physics Letters*, vol. 572, pp. 101–105, 2013.

[22] M. C. Toroker, D. K. Kanan, N. Alidoust, L. Y. Isseroff, P. Liao, and E. A. Carter, "First principles scheme to evaluate band edge positions in potential transition metal oxide photocatalysts and photoelectrodes," *Physical Chemistry Chemical Physics*, vol. 13, no. 37, pp. 16644–16654, 2011.

[23] Z. Ma, Z. Yi, J. Sun, and K. Wu, "Electronic and photocatalytic properties of $Ag_3PC_4VI$ (C = O, S, Se): a systemic hybrid DFT study," *Journal of Physical Chemistry C*, vol. 116, no. 47, pp. 25074–25080, 2012.

[24] A. J. Read and R. J. Needs, "Calculation of optical matrix elements with nonlocal pseudopotentials," *Physical Review B*, vol. 44, no. 23, pp. 13071–13073, 1991.

[25] R. M. Sheetz, I. Ponomareva, E. Richter, A. N. Andriotis, and M. Menon, "Defect-induced optical absorption in the visible range in ZnO nanowires," *Physical Review B: Condensed Matter and Materials Physics*, vol. 80, no. 19, Article ID 195314, 4 pages, 2009.